[Rock and Soil Mechanics](https://rocksoilmech.researchcommons.org/journal)

Volume 42 | Issue 3 Article 3

7-28-2021

Prediction model for compressive strength of rock-steel fiber reinforced concrete composite layer

Meng CHEN
School of Resources and Civil Engineering, Northeastern University, Shenyang, Liaoning 110819, China

Xiu-wen CUI
School of Resources and Civil Engineering, Northeastern University, Shenyang, Liaoning 110819, China

Xin YAN
School of Resources and Civil Engineering, Northeastern University, Shenyang, Liaoning 110819, China

Hao WANG
Science and Technology Innovation Center of Smart Water and Resource Environment, Northeastern University, Shenyang, Liaoning 110819, China

See next page for additional authors

Custom Citation

CHEN Meng, CUI Xiu-wen, YAN Xin, WANG Hao, WANG Er-lei, . Prediction model for compressive strength of rock-steel fiber reinforced concrete composite layer[J]. Rock and Soil Mechanics, 2021, 42(3): 638-646.

Rock and Soil Mechanics 2021 42(3): 638−646 ISSN 1000−7598
https: //doi.org/10.16285/j.rsm.2020.5571 rocksoilmech.researchcommons.org/journal

Prediction model for compressive strength of rock-steel fiber reinforced concrete composite layer

CHEN Meng[1], CUI Xiu-wen[1], YAN Xin[1], WANG Hao[2], WANG Er-lei[3]

1. School of Resources and Civil Engineering, Northeastern University, Shenyang, Liaoning 110819, China
2. Science and Technology Innovation Center of Smart Water and Resource Environment, Northeastern University, Shenyang, Liaoning 110819, China
3. Design & Research Institute of Wuhan University of Technology, Wuhan, Hubei 430070, China

Abstract: To study the uniaxial compressive strength calculation method of rock-steel fiber reinforced concrete (R-SFRC) composite layer, uniaxial compression test was carried out on rock, steel fiber reinforced concrete and R-SFRC composite layer specimens. The influence of concrete strength grades (C30, C40 and C50) and fiber contents (0, 40, 60 and 80 kg/m^3) on the uniaxial compressive strength of steel fiber reinforced concrete and composite layers was analyzed. RFPA2D was utilized to simulate the damage process and stress-strain curve of the composite layer under uniaxial compression. The compressive strength prediction model of R-SFRC composite layer was established based on Mohr-Coulomb yield criterion. The results showed that the uniaxial compressive strength for composite layer specimens was between the compressive strength of rock and concrete. The mutual restriction of rock and concrete interface in the composite layer changes the stress state of each layer. The strength of rock in the composite layer decreases while the strength of concrete increases. The ultimate compressive strength of composite layer is the strength of concrete in the composite layer. The compressive strength of composite layer specimen increases with increasing concrete matrix strength and steel fiber content, and effect of concrete matrix strength was more significant. For the uniaxial compressive strength of composite layers of different materials, the error ranges of the numerical simulation value and theoretical calculation value relative to the experimental value are −5.41%～−0.69% and −8.67%～−1.21% respectively. Numerical simulation and theoretical calculation models can be used for uniaxial compressive strength prediction of composite layers.

Keywords: rock; steel fiber reinforced concrete; composite layer; compressive strength; numerical simulation; Mohr-Coulomb yield criterion

1 Introduction

The stability control of underground engineering caverns surrounding rock is related to the safety of construction equipment and personnel, and the scientific design of supporting system is key to high-stress underground engineering[1−2]. Steel fiber reinforced concrete is widely used in the surrounding rock support structure of tunnels, roadways and slopes due to its excellent mechanical properties[3−5]. In continuous surrounding rock, the steel fiber reinforced concrete shotcrete is combined with the surrounding rock (Rock-steel fiber reinforced concrete composite layer) and provide support resistance as a whole[6]. Under the action of axial compression, the rock layer and steel fiber reinforced concrete layer interact through the interface, which affects the compressive performance of the composite layer[7]. The interaction mechanism and strength prediction model of rock and steel fiber reinforced concrete can provide a theoretical basis for the supporting structure design optimization.

Some researches have conducted experimental studies on the shear and compressive properties of rock-concrete composite specimens[8−11], and the results show that the uniaxial compressive strength of composite specimens is between rock and concrete. Xiang et al.[12] studied the macroscopic mechanical properties and microscopic failure mechanism of rock-shotcrete composite specimens through freeze−thaw cycles, uniaxial and triaxial compression, and established a damage softening statistical constitution model of the composite specimens before and after the freeze−thaw cycle. Selcuk et al.[13] studied the strength and failure behavior of rock-concrete composite specimens through uniaxial compression and split tensile tests, and discussed the influence of interface inclination angle on the strength and damage mode of the composite layer. Guo et al.[14] used the split Hopkinson pressure bar to perform dynamic compression tests on the shotcrete−surrounding rock composite, and they found

Received: 8 May 2020 Revised: 25 December 2020
This work was supported by Fundamental Research Funds for the Central Universities (N2001005), the Natural Science Foundation of Liaoning Province (2020-MS-089) and the National Training Program of Innovation and Entrepreneurship for Undergraduates(S202010145082).
First author: CHEN Meng, male, born in 1981, PhD, Associate Professor, research interests: concrete and rock dynamic mechanical properties. E-mail: chenmeng@mail.neu.edu.cn
Corresponding author: WANG Er-lei, born in 1978, PhD, Charted Engineer, research interests: dynamic properties of FRP. E-mail: wangerlei@whut.edu.cn

that the composite layer strength is related to the age of concrete and the loading rate. The bonding and friction of the interface cause mutual restraint between rock and concrete under axial load[15], which changes the stress state of rock and concrete. It is necessary to establish a composite layer compressive strength prediction model based on theoretical and experimental research.

Regarding the research of theoretical model on the “rock-rock” and “concrete-concrete” composite compressive strength, Xiao et al.[16] and Xie et al.[17] analysed the stress–strain curve and Mohr-Coulomb envelope of the “rock-rock” composite body, and established the strength model of composite rock mass under unidirectional stress state. Qin et al.[18] conducted direct shear tests and double-edge notched single-edge compressing tests on the interfacial properties of layered concrete, and established a fracture toughness prediction model based on the Mohr-Coulomb yield criterion. Based on the two-parameter Mohr-Coulomb yield criterion, Domingo et al.[19] established a stress–strain model suitable for FRP-confined concrete under uniaxial and triaxial compression loading conditions. Other related research shows that the Mohr-Coulomb yield criterion can be used to study the strength model of layered rock or concrete materials under axial load.

Chinese scholars have conducted numerical simulation on the failure process of rock materials. Tang et al.[20] used the elastic damage theory and Weibull distribution to describe the distribution characteristics of compressive strength and elastic modulus of rock meso-units and developed the RFPA2/3D model. Xu et al.[21] compared the numerical simulation and test results of rock samples under uniaxial conditions, and found that the numerical simulation curve is in good agreement with the linear, near-peak and post-peak sections of the test curve. Huang et al.[22] analyzed the numerical simulation and experimental results of a single-cracked rock specimen failure under uniaxial loading, and showed that RFPA2D can simulate the crack propagation process of brittle materials. Lu et al.[23] employed RFPA software to study the wing crack model of concrete materials. RFPA2D can perform numerical simulation on the rock and concrete materials properties, and can well reflect the strength, deformation, and damage process of the material.

In this study, steel fiber reinforced concrete with different matrix strength (C30, C40, C50) and different fiber contents (0, 40, 60, 80 kg/m³) are designed, and uniaxial compression test on rock, steel fiber reinforced concrete and rock-steel fiber reinforced concrete composite layers are conducted to examine mechanical parameters such as elastic modulus, Poisson's ratio and internal friction angle of rock and steel fiber reinforced concrete. The uniaxial compressive strength and failure process of composite layer specimens are simulated by RFPA2D. Based on the Mohr-Coulomb yield criterion, the compressive strength prediction model of the rock-steel fiber reinforced concrete composite layer is constructed.

2 Test overview

2.1 Preparation of concrete specimens

The P·O42.5 ordinary Portland cement is adopted in test. Fine aggregate of natural river sand with the maximum particle size of 4.75 mm is used with a fineness modulus of 2.56. The coarse aggregate is crushed granite with a particle size of 5–10 mm and good gradation. The water reducing agent is polycarboxylic acid with a reduction rate of 38%. The steel fiber is Dramix 3D 65/35BG end hook type fiber produced by Shanghai Bekaert Company. The morphology, physical and mechanical properties of the steel fiber are listed in the Table 1 and the mix ratios of different types of concrete are provided in Table 2.

Table 1 Physical and mechanical properties of steel fiber

Fiber morphology	Elastic Modulus /GPa	Density /(kg • m^{-3})	Length /mm	Aspect ratio
	220	7 850	35	65

The cement and aggregate are placed in a mixer for mixing according to the mixing ratio, then water and water reducing agent are added for wet mixing, the mixing time is no less than 2 minutes, and the steel fiber is finally put in and stirred until the fiber is evenly distributed. The concrete mixture is poured into mold to make a cubic test block with a side length of 150 mm (cubic compressive strength test), cylindrical test specimen with a diameter of 100 mm and a height of 50 mm (cylinder compressive strength test), cylindrical test specimen with a diameter of 50 mm and a height of 100 mm (direct shear test) and prism test block with a size of 150 mm × 150 mm × 300 mm (elastic modulus and Poisson's ratio test). After vibrating and compacting, the samples are covered with plastic wrap, demoulded after 24 hours and put into a standard curing room (temperature 20 ℃ ± 2 ℃, relative humidity above 95%) to cure for 28 days.

2.2 Preparation of rock and composite layer specimens

The granite used in test is processed into cylinder

https://rocksoilmech.researchcommons.org/journal/vol42/iss3/3
DOI: 10.16285/j.rsm.2020.5571

Table 2 Mixture proportions of steel fiber reinforced concrete and test results

Sample No	Cement content /(kg • m^{-3})	Fine aggregate content /(kg • m^{-3})	Coarse aggregate content /(kg • m^{-3})	Water content /(kg • m^{-3})	Water-reducing admixture content /(kg • m^{-3})	Steel fiber content /(kg • m^{-3})	f_C /MPa	f'_C /MPa	Elastic modulus E_C /GPa	Poisson's ratio μ_C	Internal friction angle /(°)
C30S0	268	728	1 293	161	2.68	0	32.8	39.9	31.3	0.231	35.5
C30S4	268	728	1 293	161	2.68	40	33.4	40.8	31.7	0.225	36.6
C30S6	268	728	1 293	161	2.68	60	34.0	41.7	31.9	0.221	37.9
C30S8	268	728	1 293	161	2.68	80	34.8	42.6	32.4	0.219	38.3
C40S0	418	611	1 239	182	4.18	0	38.5	47.0	32.7	0.226	35.9
C40S4	418	611	1 239	182	4.18	40	39.4	48.3	33.1	0.221	37.1
C40S6	418	611	1 239	182	4.18	60	40.4	49.2	33.8	0.218	38.3
C40S8	418	611	1 239	182	4.18	80	41.5	50.8	34.2	0.214	39.1
C50S0	500	674	1 100	155	5.00	0	53.5	63.9	35.3	0.221	36.2
C50S4	500	674	1 100	155	5.00	40	55.4	66.1	35.5	0.213	37.9
C50S6	500	674	1 100	155	5.00	60	56.8	68.3	36.1	0.211	38.7
C50S8	500	674	1 100	155	5.00	80	58.9	71.3	36.8	0.207	39.2

Note: C30S4 indicates that the concrete strength grade is C30, the steel fiber content is 40 kg/m^3, and so on, f_C and f'_C are the uniaxial compressive strength of concrete cube and cylindrical specimens, respectively.

specimens with a diameter of 50 mm and a height of 100 mm (for uniaxial compression and direct shear tests) and a diameter of 100 mm and a height of 50 mm (for uniaxial compression and composite layer specimens) after core drilling, cutting, and grinding. The non-parallelism of the two ends of the cylindrical specimen should be less than 0.1% of the diameter, and the deviation between the two ends and the axis should not be more than 0.25°. The mechanical properties of granite are tested according to *Standard for test methods of engineering rock masses* (GB/T50266-2013)[24], and the physical and mechanical properties of granite are shown in Table 3.

Table 3 Physical and mechanical properties of rock

Density /(kg • m^{-3})	Elastic modulus E_R / MPa	f_R /MPa	f'_R /MPa	Poisson's ratio μ_R	Internal friction angle /(°)
3 000	67.41	158.5	187.1	0.207	53

Note: f_R and f'_R are the uniaxial compressive strength of cylindrical specimens with a diameter of 50 mm, a height of 100 mm, and a diameter of 100 mm, and a height of 50 mm, respectively.

When preparing the rock-steel fiber reinforced concrete (R-SFRC) composite layer specimen, the concrete mixture is poured into a cylindrical mould first with a diameter of 100 mm and a height of 50 mm, and then the surface wetted rock specimens is affixed onto the surface of the cylindrical concrete specimen after vibrating, the mortar on the upper part of the concrete specimen tightly bonds the interface between the rock and concrete. The rock is placed onto the upper part of the concrete specimen. After 24 hours, the concrete mould is removed and specimen is then placed in a standard curing room for 28 d curing. There are in total 12 types of composite layer specimens bonded between rock and different types of concrete, and the numbers are shown in Table 2. The R-SFRC composite layer test specimen is shown in Fig. 1.

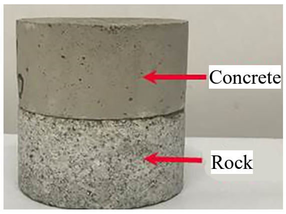

Fig. 1 Composite layer specimen

3 Test results and discussion

3.1 Test results of steel fiber reinforced concrete

The variation of cubic concrete compressive strength with steel fiber content is shown in Fig. 2. The cubic compressive strengths of C30S0, C40S0 and C50S0 are 32.8, 38.5 and 53.5 MPa, respectively. The cubic compressive strengths of C30S4, C30S4, and C30S6 increase by 1.8%, 3.6%, and 6.1% relative to C30S0, respectively. The cubic compressive strengths of C40S4, C40S6, and C40S8 increase by 2.3%, 4.9%, and 7.7%, respectively, relative to C40S0. Compared with C50S0, the cubic compressive strengths of C50S4, C50S6 and C50S8 grow by 3.6%, 6.2% and 10.0%, respectively. The cubic compressive strength of specimens with the same strength grade increases with increasing steel fiber content. And when the steel fiber content is constant, the cubic compressive strength increases with increasing matrix strength. The reason is that there are internal cracks in the concrete under compression, and the steel fiber interacts with the concrete matrix to play a "bridging" role in the expansion of the crack. The higher the concrete matrix strength, the greater the bonding and anchoring force between the steel fiber and the matrix, and the greater the increase of concrete cubic compressive strength.

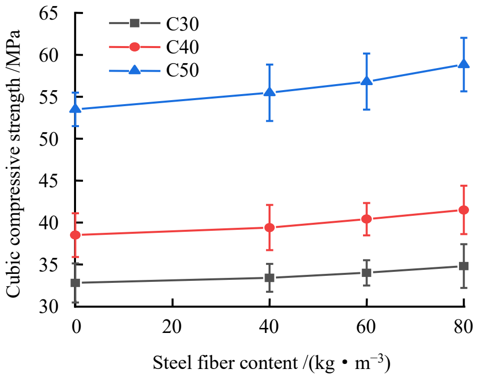

Fig. 2 Compressive strength of cubic steel fiber reinforced concrete

The elastic modulus, Poisson's ratio and direct shear test results of different types of concrete are shown in Table 2. When the strength of concrete matrix is constant, the elastic modulus increases with increasing steel fiber content, and the Poisson's ratio decreases. The reason is that the steel fiber with high elastic modulus restrains the lateral expansion and reduce the transverse strain of the specimen[25]. The internal friction angle of concrete increases with increase of compressive strength and steel fiber content, and the steel fiber content has a greater influence on the internal friction angle. The internal friction angle of different concrete types ranges from 35.5° to 39.2°. Previous literatures[26–27] reported a calculation formula for the change of internal friction angle with uniaxial compressive strength as

$$\varphi_{C} = 36^{\circ} + 1^{\circ}\frac{f_{C}}{35} \leqslant 45^{\circ} \quad (1)$$

where φ_{C} is the internal friction angle of concrete.

Equation (1) shows that the internal friction angle of concrete increases with increasing concrete uniaxial compressive strength. Literature [28] shows that the internal friction angle of concrete with different strengths does not change much, and the range of concrete internal friction angle is 30°–35°. Literature [29] reported the internal friction angle of concrete with cubic compressive strength of 14.4–47.0 MPa is between 29.8° and 38.6° through experiments. It can be seen that there are many factors influencing the internal friction angle of concrete, but the range of change is relatively small.

3.2 Compressive strength of R-SFRC composite layer

The uniaxial compressive strength values f_{CR}^{e} of R-SFRC composite layer specimens are summarized in Table 4. When the strength of concrete matrix is constant, the compressive strength of R-SFRC composite layer increases with increasing steel fiber content. When the fiber content increases from 40 kg/m^3 to 80 kg/m^3, the R-SFRC composite layer uniaxial compressive strength of the specimen is increased by 1.96%–11.33% compared with the plain concrete composite layer specimen. When the steel fiber content is constant, the uniaxial compressive strength of composite layer specimen increases with the increase of the concrete matrix strength, with R-C50S0 being 45.50% and 27.55% larger than R-C30S0 and R-C40S0, respectively; R-C50S4 being 45.10% and 24.18% larger than R-C30S4 and R-C40S4, respectively; R-C50S6 being larger than R-C30S6 and R-C40S6 by 46.71% and 26.32%, respectively; and R-C50S8 increasing 45.33% and 24.36% from R-C30S8 and R-C40S8, respectively. The uniaxial compressive strength of composite layer is between the compressive strength of concrete and rock. This result is contributed to the fact that the composite layer specimen experiences compression deformation under the action of axial loading, the elastic modulus of concrete is smaller than that of rock and the Poisson's ratios of the two layers are close, the axial and circumferential deformations of the concrete layer are larger than those of the rock layer. The two-layer interface maintains close contact during compression, and the concrete and

Table 4 Uniaxial compressive strength of composite layer specimens

Sample No.	f_{CR}^{e} /MPa	f_{CR}^{a} /MPa	f_{CR}^{t} /MPa	x_a /%	x_t /%
R-C30S0	61.1	58.6	55.8	−4.16	−8.67
R-C30S4	62.3	60.8	58.2	−2.36	−6.58
R-C30S6	63.8	61.9	58.6	−2.99	−8.15
R-C30S8	66.4	63.5	62.8	−4.37	−5.42
R-C40S0	69.7	66.5	65.8	−4.58	−5.60
R-C40S4	72.8	70.8	69.0	−2.76	−5.22
R-C40S6	74.1	71.2	73.2	−3.97	−1.21
R-C40S8	77.6	73.4	75.7	−5.41	−2.45
R-C50S0	88.9	87.3	85.8	−1.80	−3.49
R-C50S4	90.4	89.8	86.5	−0.69	−4.31
R-C50S6	93.6	92.3	90.2	−1.35	−3.63
R-C50S8	96.5	95.8	93.2	−0.77	−3.42

Note: x_a and x_t are the deviations of the simulated value f_{CR}^{a} and calculated value f_{CR}^{t} to the tested uniaxial compressive strength value of the composite layer specimens, respectively, $x_a = \frac{f_{CR}^{a} - f_{CR}^{e}}{f_{CR}^{e}} \times 100\%$ and $x_t = \frac{f_{CR}^{t} - f_{CR}^{e}}{f_{CR}^{e}} \times 100\%$.

rock are mutually restrained at the interface, causing the concrete and rock near the interface to be subjected to lateral compression and tension, respectively. According to the Mohr strength theory, the strength of rock under lateral tension decreases, and the strength of concrete under lateral compression increases.

4 Numerical simulation of failure process

4.1 Numerical simulation model

RFPA2D is utilized to build a rock-concrete composite layer model. The Weibull distribution is used to describe the distribution characteristics of uniaxial compressive strength and elastic modulus of the meso-elements. The calculation formulas for the micro-strength value and the micro-elastic modulus value are as follows:

$$\left.\begin{aligned}\frac{f_{cs}}{f_{cs0}} &= 0.260\,2\ln m + 0.023\,3\\ \frac{E_s}{E_{s0}} &= 0.141\,2\ln m + 0.647\,6\end{aligned}\right\} \quad (2)$$

where f_{cs0} and E_{s0} are the mean values of micro-strength and the micro-elastic modulus when the Weibull distribution is assigned; f_{cs} and E_s are the macro-strength and the micro-elastic modulus of the specimen, respectively, and m is the degree of homogeneity.

The calculation model mesh is divided by the structured generation method, the model size is 100 mm×100 mm, the cell size is 1 mm×1 mm, and 120 mm×10 mm loading platens are set above and below (loading platen homogeneity is set to 100), as shown in Fig. 3. The rock homogeneity is set as 1.5, the concrete homogeneity as 2, the maximum compressive strain coefficient as 200, the maximum tensile strain coefficient as 1.5, the residual strength percentage as 0.1, and the residual Poisson percentage as 0.1. The numerical calculation model parameters are shown in Table 5. The simplified model is a plane stress model, and the failure criterion utilizes the Mohr-Coulomb yield criterion. The loading process is vertical displacement loading, and the loading amount per step is 0.002 mm.

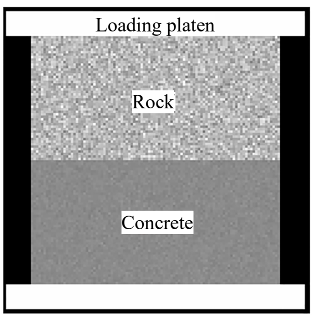

Fig. 3 Model schematic of composite layer specimen

Table 5 Mechanical parameter assignment and calculation results

Material	f_{cs0} / MPa	E_{s0} / MPa	compressive-tensile ratio	Reduction factor k
Loading platens	10 000.0	200 000	1.0	—
Granite	1 452.3	95 637	10.0	—
C30S0	195.8	41 987	10.0	0.637
C30S4	200.4	42 523	9.6	0.680
C30S6	204.5	42 792	9.4	0.647
C30S8	209.0	43 462	9.2	0.737
C40S0	230.8	43 865	11.0	0.686
C40S4	237.0	44 401	10.6	0.729
C40S6	241.8	45 340	10.4	0.793
C40S8	249.2	45 877	10.2	0.815
C50S0	313.9	47 353	12.0	0.695
C50S4	324.5	47 621	11.6	0.653
C50S6	335.2	48 426	11.4	0.679
C50S8	350.2	49 365	11.2	0.690

4.2 Analysis of numerical results

The stress−strain simulation curves of composite layer specimen under uniaxial compression are shown in Fig. 4, and the compressive strength simulation values are listed in Table 4. In the initial stage, the stress increases linearly with strain. After entering the elastoplastic stage, the stress drops slightly and then rises. The reason for this is that the edge of concrete layer is damaged, and the central area strength keeps growing due to the interface constraints, so can continue to bear the load. After reaching the ultimate strength, stress steeply descends in a "multi-step" manner. In this progress, the internal cracks in the concrete layer gradually coalesce and extend to the rock layer through the interface. As a result, the composite layer specimen is completely destroyed.

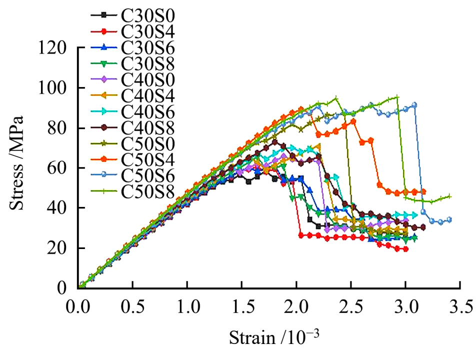

Fig. 4 Stress−strain curves of composite layer specimens

The simulated uniaxial compressive strength of the composite layer specimen is less than the tested value. The differences between the simulated and the tested values of compressive strength of R-SFRC(C30, C40 and C50) composite layers are −4.37% to −2.36%, −5.41%

to −2.76% and −1.80% to −0.69%, respectively. The reason is that the unit body will undergo stiffness degradation treatment in the later stage of numerical simulation failure process[18], but in the actual test, the material micro-element does not completely withdraw from work after the failure and can still bear part of the stress.

4.3 Failure mode of composite layer specimens

Figures 5 and 6 show the failure diagrams of specimens from numerical calculation and uniaxial compression test (taking C40 concrete as an example), respectively. Numerical calculations show that there are oblique cracks inside the concrete of composite layer specimens. Affected by the interface constraints, vertical cracks appear at the edges of the concrete, and finally spalling failure occurs and the concrete cracks extend through the interface to the rock layer. Figure 6(a) presents the failure mode of the composite layer specimen without steel fiber. The rock layer has almost no damage but the concrete layer is broken along circumference, which is characterized by brittle failure. As seen in Figs.6(b)−(d), the multiple vertical and longitudinal cracks occur in rock layer of R-SFRC; cracking and flaking appear at the edges of the steel fiber reinforced concrete layer, showing the ductile failure characteristics of the overall collaborative deformation. The number of cracks in the concrete layer declines as the amount of steel fiber increases

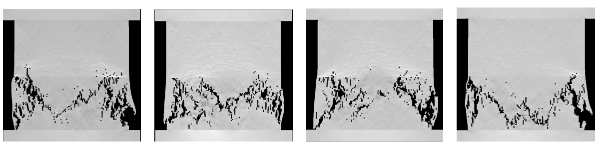

(a) R-C40S0 (b) R-C40S4 (c) R-C40S6 (d) R-C40S8

Fig. 5 Failure of specimen in numerical calculation

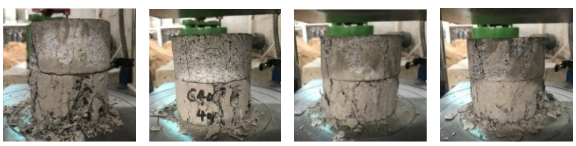

(a) R-C40S0 (b) R-C40S4 (c) R-C40S6 (d) R-C40S8

Fig. 6 Failure of specimen under test

5 Prediction model

5.1 Stress analysis of the unit body at the interface of the R-SFRC composite layer

Because the elastic modulus and Poisson's ratio of the two materials in the composite layer are different, the axial and circumferential deformations produced in the two layers under the action of axial loading are different. From the analysis in section 3.2, it can be seen that the bonding interface of composite layer is mutually restraint, which incurs compressive and tensile stresses in the lateral direction, respectively in concrete and the rock. Take the unit body at the interface for analysis, which is shown in Fig. 7.

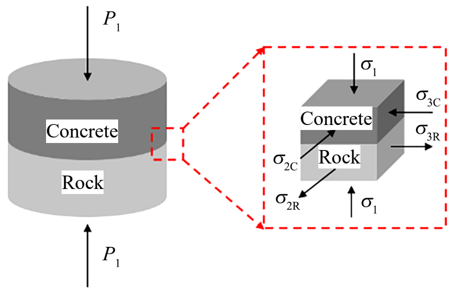

Fig. 7 Stress analysis diagram of unit body at composite layer specimen interface

Assuming that the interface of composite layer remains in close contact during compression and the compressive stress and tensile strain are specified to be positive values. The relationship between the continuous deformation and static equilibrium conditions of the three-dimensional unit body of the variable elastic modulus in Fig. 7 is[30]

$$\varepsilon_{2C} = \varepsilon_{3C} = \varepsilon_{2R} = \varepsilon_{3R} \tag{3}$$

$$\sigma_{2C} = \sigma_{3C} = -\sigma_{2R} = -\sigma_{3R} \tag{4}$$

where ε_{2C} and ε_{3C} are the strains of concrete in the 2 and 3 directions, respectively; ε_{2R} and ε_{3R} are the strains of rock in the 2 and 3 directions, respectively. σ_{2C} and σ_{3C} are the stresses of concrete in the 2 and 3 directions, respectively and σ_{2R} and σ_{3R} are the stresses of rock in the 2 and 3 directions, respectively.

According to the generalized Hooke's law, it is known that:

$$\left.\begin{aligned}\varepsilon_{3R} &= \left[\sigma_{3R} - \mu_R\left(\sigma_1 + \sigma_{2R}\right)\right] / E_R \\ \varepsilon_{3C} &= \left[\sigma_{3C} - \mu_C\left(\sigma_1 + \sigma_{2C}\right)\right] / E_C\end{aligned}\right\} \tag{5}$$

Combining Eqs. (3)−(5), we have

$$\sigma_{3C} = -\sigma_{3R} = \frac{\left(E_R\mu_C - E_C\mu_R\right)}{\left[E_C\left(1-\mu_R\right) + E_R\left(1-\mu_C\right)\right]}\sigma_1 \tag{6}$$

let

$$a = \frac{\left(E_R\mu_C - E_C\mu_R\right)}{\left[E_C\left(1-\mu_R\right) + E_R\left(1-\mu_C\right)\right]} \tag{7}$$

such that

$$\sigma_{3C} = -\sigma_{3R} = a \cdot \sigma_1 \tag{8}$$

5.2 R-SFRC composite layer compressive strength modeling

The normal stress σ and shear stress τ in any plane

I–I in a material element body (see Fig. 8) are:

$$\sigma=\frac{1}{2}(\sigma_1+\sigma_3)+\frac{1}{2}(\sigma_1-\sigma_3)\cos(2\alpha) \quad (9)$$

$$\tau=\frac{1}{2}(\sigma_1-\sigma_3)\sin(2\alpha) \quad (10)$$

where σ_1 and σ_3 are the maximum principal stress and the minimum principal stress of the element body, respectively; α is the angle between the direction of the maximum principal stress and the I–I shear plane.

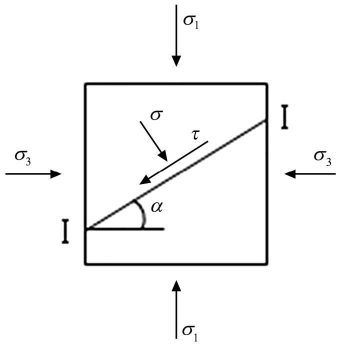

Fig. 8 Plane stress analysis diagram of material unit

The Mohr-Coulomb yield criterion is[31]

$$\tau=c+\sigma\cdot\tan\varphi \quad (11)$$

where τ is the shear strength; c is the cohesive force, and φ is the internal friction angle.

σ, τ, σ_1 and σ_3 in Eqs. (9), (10), and c and φ in Eq. (11) can be represented by the Mohr circle shown in Fig. 9, then:

$$2\alpha=90^{\circ}+\varphi \quad (12)$$

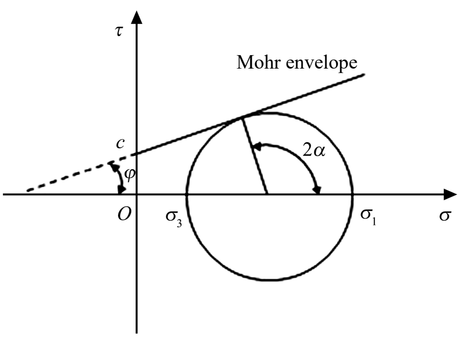

Fig. 9 Mohr envelope

Combining Eqs. (9)–(12) yields the equilibrium state equation of ultimate stress under two-dimensional stress[32]:

$$\sigma_1=\frac{1+\sin\varphi}{1-\sin\varphi}\sigma_3+\frac{2c\cos\varphi}{1-\sin\varphi} \quad (13)$$

When the material is under uniaxial compression $\sigma_3=0$, the uniaxial compressive strength f of the material is obtained:

$$f=\sigma_1=\frac{2c\cos\varphi}{1-\sin\varphi} \quad (14)$$

The interface of the composite layer is mutually constrained, and the rock and the concrete layers are in a three-way stress state, thus, Eq. (13) can be converted into

$$\sigma_1=\frac{1+\sin\varphi}{1-\sin\varphi}\sigma_3+f \quad (15)$$

Let $k_{\rm R}=\frac{1+\sin\varphi_{\rm R}}{1-\sin\varphi_{\rm R}}$, where $\varphi_{\rm R}$ is the friction angle of the rock, and substitute Eq. (8) into Eq. (15), the compressive strength of the rock in the composite layer specimen can be obtained:

$$f_{\rm CR-R}=\sigma_1=\frac{f'_{\rm R}}{1+a\cdot k_{\rm R}} \quad (16)$$

In the same way, the compressive strength of concrete in the composite layer specimen is

$$f_{\rm CR-C}=\sigma_1=\frac{f'_{\rm C}}{1-a\cdot k_{\rm C}} \quad (17)$$

Obviously, $f_{\rm CR-R}<f'_{\rm R}$ and $f_{\rm CR-C}>f'_{\rm C}$, therefore, the compressive strength of the composite layer specimen $f^{\rm t}_{\rm CR}$ is

$$f^{\rm t}_{\rm CR}=\min\{f_{\rm CR-R}, f_{\rm CR-C}\} \quad (18)$$

5.3 Modification of the compressive strength prediction model of R-SFRC composite layer

In the uniaxial compression test, the interface between rock and concrete layers is mutually constrained, and the confinement effect of the center and edge area are different, so the stress at different positions of the interface is different. In the numerical results, the ratio of minimum principal stress to maximum principal stress of the unit body at the interface a' is counted. The result shows that there is a difference between a' and test obtained a, so the reduction factor k (ratio of a' to a) is introduced. The value of k is shown in Table 5. Equation (8) can be expressed as

$$\sigma'_{\rm 3C}=-\sigma'_{\rm 3C}=k\cdot a\cdot\sigma_1 \quad (19)$$

The revised theoretical calculation value of composite layer compressive strength $f^{\rm t}_{\rm CR}$ is listed in Table 4. The calculated compressive strength of rock in composite layer specimen is 94.0–107.6 MPa, which is 59.32%–67.91% less than the uniaxial compressive strength of the single-layer rock specimen. The calculated value of concrete compressive strength in the composite layer specimen is 58.6–95.8 MPa. The uniaxial compressive strength is increased by 30.65%–49.21% compared with single-layer concrete specimens. It can be seen from $f_{\mathrm{CR-R}} > f_{\mathrm{CR-C}}$ and the damage pattern of specimen that the damage of the composite layer specimen is caused by the concrete reaching the ultimate compressive strength first, and the theoretical calculation value of composite layer strength is the compressive strength of concrete in the composite layer specimen. The error of theoretical calculation value of the composite layer's uniaxial compressive strength relative to the experimental value is between −8.67% and −1.21%, which indicates that the theoretical calculation formula can predict the uniaxial compressive strength of the composite layer specimen more accurately.

6 Conclusion

(1) The uniaxial compressive strength of the composite layer formed by bonding different types of steel fiber reinforced concrete to rock is between those of rock and concrete, and is closer to the strength of concrete. The compressive strength of composite layer increases with increasing concrete strength and amount of steel fiber.

(2) Numerical simulation results show that there are oblique cracks inside the concrete in the composite layer. Affected by the interface constraints, vertical cracks appear at the edges of the concrete, and finally spalling failure occurs. The spalling damage of concrete in the composite layer specimen decreases with increasing strength grade. The numerical result of the composite layer's uniaxial compressive strength is less than the experimental value, with an error of −5.41% to −0.69%.

(3) Based on the Mohr-Coulomb yield criterion, the compressive strength prediction model of R-SFRC composite layer under axial load is developed. The results show that the rock strength in the composite layer is lower than the uniaxial compressive strength in the test, and the concrete strength is higher than that in the test. The theoretical calculation value of the composite layer's uniaxial compressive strength is less than the experimental value, and the error is −8.67% to −1.21%. This model can be used to predict the compressive strength of the rock-concrete composite layer.

References

[1] JIANG Quan, FENG Xia-ting, LI Shao-jun, et al. Cracking-restraint design method for large underground caverns with hard rock under high geostress condition and its practical application[J]. Chinese Journal of Rock Mechanics and Engineering, 2019, 38(6): 1081−1101.

[2] JIANG Quan, HOU Jing, FENG Xia-ting, et al. Dynamic feedback analysis and engineering control of surrounding rock local instability in underground powerhouse of Jinping II hydropower station[J]. Chinese Journal of Rock Mechanics and Engineering, 2008, 27(9): 1899−1907.

[3] MONCEF L N, SAFEER A, AHMED M S. Exploratory study of ultra-high performance fiber reinforced concrete tunnel lining segments with varying steel fiber lengths and dosages[J]. Engineering Structures, 2015, 101: 733−742.

[4] MOHAMMAD J A. Response modification factors for seismic design of steel fiber reinforced concrete segmental tunnels[J]. Construction and Building Materials, 2019, 211: 1042−1049.

[5] LIU Xin-rong, ZHU Yun-hua, LI Xiao-hong, et al. Experimental research on single-layer tunnel lining of steel fiber shotcrete[J]. Rock and Soil Mechanics, 2009, 30(8): 2319−2323.

[6] GUO D M, YAN P Y, FAN L F. Experimental study on dynamic mechanical properties of sprayed concrete-surrounding rock combined body[J]. Journal of Beijing Institute of Technology, 2019, 28(2): 278−285.

[7] PRIYANKA J, TANUSREE C. Numerical analysis of tunnel in rock with basalt fiber reinforced concrete lining subjected to internal blast load[J]. Computers and Concrete, 2018, 21(4): 399−406.

[8] LIU Hai-feng, ZHU Chang-qi, WANG Ren, et al. Shear test on reef limestone-concrete bonding interface[J]. Rock and Soil Mechanics, 2020, 41(5): 1540−1548.

[9] ZENG Sheng, ZHANG Ni, SUN Bin, et al. Mechanical performance of uni-body bi-material model for rock-concrete under dry and saturated states[J]. Bulletin of the Chinese Ceramic Society, 2018, 37(7): 2206−2209, 2213.

[10] ZHAO B Y, LIU Y, HUANG T Z, et al. Experimental study on strength and deformation characteristics of rock-concrete composite specimens under compressive condition[J]. Geotechnical and Geological Engineering, 2019, 37(4): 2693−2706.

[11] SU Hui, ZHANG Yu-ting, LI Qi, et al. Acoustic emission test of rock-concrete integrated two-body medium combined with discrete element method[J]. Science Technology and Engineering, 2019, 19(23): 206−210.

[12] XIANG Wei, LIU Xun. Experimental study on mechanical

DOI: 10.16285/j.rsm.2020.5571

properties of rock shotcrete composite specimens under freeze-thaw cycles[J]. Chinese Journal of Rock Mechanics and Engineering, 2010, 29(12): 2510−2521.

[13] SELCUK L, ASMA D. Experimental investigation of the rock-concrete bi materials influence of inclined interface on strength and failure behavior[J]. International Journal of Rock Mechanics and Mining Sciences, 2019, 123(11): 1365−1609.

[14] GUO Dong-ming, YAN Peng-yang, ZHANG Ying-shi, et al. Experimental research on the sprayed concrete-surrounding rock combined body subjected to cyclic impact loading[J]. Journal of Vibration and Shock, 2019, 38(10): 105−111.

[15] MOUZANNAR H, BOST M, LEROUX M, et al. Experimental study of the shear strength of bonded concrete-rock interfaces: surface morphology and scale effect[J]. Rock Mechanics and Rock Engineering, 2017, 50(10): 2601−2625.

[16] XIAO Chang-fu, QIU Xian-de. Discussion on strength and deformation characteristics of composite rock under uniaxial and triaxial compression stress[J]. Journal of Chongqing University, 1983(3): 23−39.

[17] XIE He-ping, CHEN Zhong-hui, ZHOU Hong-wei, et al. A preliminary study of two physical mechanics models based on the interaction between engineering body and geological body[J]. Chinese Journal of Rock Mechanics and Engineering, 2005, 24(9): 1457−1464.

[18] QIN Qian, XU Qian-jun. The shear strength and mode II fracture toughness of layered concrete[J]. Engineering Mechanics, 2019, 36(9): 188−196.

[19] DOMINGO A M, CHRIS P P. Elliptical and circular FRP-confined concrete sections: a Mohr-Coulomb analytical model[J]. International Journal of Solids and Structures, 2012, 49(6): 881−898.

[20] TANG C A, THAM L G, LEE P K K, et al. Numerical studies of the influence of microstructure on rock failure in uniaxial compression—part II: constraint, slenderness and size effect[J]. International Journal of Rock Mechanics and Mining Sciences, 2000, 37(4): 571−583.

[21] XU Tao, TANG Chun-an, ZHANG Zhe, et al. Theoretical, experimental and numerical studies on deformation and failure of brittle rock in uniaxial compression[J]. Journal of Northeastern University (Natural Science), 2003, 24(1): 87−90.

[22] HUANG Ming-li, TANG Chun-an, ZHU Wan-cheng. Numerical simulation on failure process of rock[J]. Chinese Journal of Rock Mechanics and Engineering, 2000, 19(4): 468−471.

[23] LU Yu-bin, ZHU Wan-cheng. Comparison of wing crack models for concrete-like materials and RFPA numerical simulation verification[J]. Concrete, 2013, 289(11): 32−36.

[24] China Electricity Council. GB/T 50266—2013 Standard for test methods of engineering rock mass[S]. Beijing: China Planning Press, 2013.

[25] HE Dong-qing, LU Chang. Experimental study on elastic modulus and Poisson’s ratio of several fiber reinforced concretes[J]. Architecture Technology, 2015, 46(1): 50−52.

[26] LI Y F, LIN C T, SUNG Y Y. A constitutive model for concrete confined with carbon fiber reinforced plastics[J]. Mechanics of Materials, 2003, 35(3): 603−619.

[27] GOODMAN R E. Introduction to rock mechanics[M]. New York: Wiley Press, 1989.

[28] VERMEER P A, RENE D B. Non-associated plasticity for soils[J]. Rete and Rock, 1984, 29: 1−64.

[29] SELIM P, AMIR G, ERTEKIN O, et al. Experimental determination of cohesion and internal friction angle on conventional concretes[J]. ACI Structural Journal, 2017, 114(3): 407−416.

[30] XIAN Xue-fu, TAN Xue-shu. Layered rock failure mechanism[M]. Chongqing: Chongqing University Press, 1989.

[31] ZHAO J. Applicability of Mohr-Coulomb and Hoek-Brown strength criteria to dynamic strength of brittle rock materials[J]. International Journal of Rock Mechanics and Mining Sciences, 2000, 37(7): 1115−1121.

[32] GONG Feng-qiang, SI Xue-feng, LI Xi-bing, et al. Study on rock dynamic Mohr-Coulomb criterion and Hoek-Brown criterion based on strain rate effect[J]. Chinese Journal of Nonferrous Metals, 2016, 26(8): 1763−1773.